Cav03-GS-9-006

Fifth International Symposium on Cavitation (CAV2003)
Osaka, Japan, November 1-4, 2003

A JOINT EXPERIMENTAL AND NUMERICAL STUDY OF MECHANISMS ASSOCIATED TO INSTABILITY OF PARTIAL CAVITATION ON TWO-DIMENSIONAL HYDROFOIL.

Jean-Baptiste Leroux[1]
leroux@ecole-navale.fr

Olivier Coutier-Delgosha[2]
coutier@enstay.ensta.fr

Jacques André Astolfi [1]
astolfi@ecole-navale.fr

(1) Institut de Recherche de l'Ecole Navale – EA3634, BP 600, 29240 BREST NAVAL, FRANCE
(2) ENSTA – UER de Mécanique, Chemin de la Hunière, 91761 Palaiseau Cedex, FRANCE

ABSTRACT

The present work was carried out in the scope of a numerical-experimental collaborative research program, whose main objective is to understand the mechanisms of instabilities in partial cavitating flow. Experiments and numerical simulations were conducted in the configuration of a 2D foil section located in a cavitation tunnel with various angles of attack. Several physical features have been pointed out by this joined approach. The role played by the re-entrant jet in the cloud shedding phenomenon was investigated at several incidences, and it was found that it is mainly responsible for the cavity break off. Moreover, a special flow pattern was evidenced for a 6° angle of attack: in that case a growth/destabilization cycle of the cavity is observed at a low frequency (~ 3.5 Hz), together with the periodic shedding of large bubble clusters (cloud cavitation).

INTRODUCTION

Unsteady cavitation is responsible for undesirable effects or even damage in hydraulic installations such as turbomachinery or naval propellers. Generally, sheet cavitation that occurs on the blade suction side of pumps generally adopts a more or less pronounced unsteady behaviour. At small angle of attack or low velocity, this phenomenon mainly affects the rear part of the cavity, while in more unfavourable conditions all the vaporized area becomes unstable, with periodical shedding of large bubble clusters. This second configuration, usually called "cloud cavitation", generates both pressure fluctuations downstream from the cavity, important vibrations, and also acoustic emission due to the bubble collapse close to the solid walls.

Cloud cavitation has been studied experimentally by many authors in two main configurations, namely Venturi type sections [Furness and Hutton, 1975, Lush and Peters, 1982, Stutz and Reboud, 1997a] and two-dimensional foil sections [Kawanami et al., 1997, Pham et al., 1999, Laberteaux and Ceccio, 2001, Leroux and Astolfi, 2003]. The recurrent question in all these papers concerns the origin of the flow instability [Arndt et al., 2000]. Up to now, most of the works point out a re-entrant jet that flows under the cavity from its rear part to its upstream end. When this jet reaches the sheet interface, the cavity breaks off and its downstream part is convected by the main flow until it collapses. This process, initially evocated by [Furness and Hutton, 1975], was more recently confirmed by measurements performed with electrical impedance probes [Pham et al., 1999] and double optical probes [Stutz and Reboud, 1997a, b]. The development of the reverse flow has led to several conjectures: it might result either from the collapse of the previous cloud of vapour [Le et al., 1993] or from a mechanism associated with the cavity growth [Furness and Hutton, 1975, de Lange et al., 1994]. Other physical processes were also found to contribute to the flow instability: [Lush and Peters, 1982] impute the cavitation sheet break-off to the combination of the re-entrant jet with a periodic interface destabilization in the rear part of the cavity.

Calculations of unsteady cavitating flow have much advanced for about ten years: several configurations of two-dimensional cloud cavitation have been accurately simulated by [Chen and Heister, 1995, Grogger and Alajbegovic, 1998, Kunz et al., 2001, Song and Qin, 2001, Lohrberg et al., 2002 Coutier-Delgosha et al., 2003a, b]. In all these studies the complete flow including the vaporized areas is computed, which avoids to set any cavity closure condition. The two-phase flow is thus considered as a single fluid characterized by variable proportions of vapour and liquid. Mass and momentum transfers between the two phases are managed either by a barotropic state law derived from the model proposed by [Delannoy and Kueny, 1990], by a supplementary equation that controls the convection/production of vapor [Kunz et al., 2001,

Merkle et al., 1998], or by the evolution of a cluster of bubbles according to a simplified Reyleigh-Plesset equation [Kubota et al., 1992].

The present work is devoted to the study of the cavitating flow on the suction side of a two-dimensional foil section. Cloud cavitation is investigated both experimentally by the IRENav cavitation team (Ecole Navale, Brest, France) and numerically with a model developed in the Turbomachinery/cavitation team of the LEGI laboratory (Grenoble, France). This joined approach intends to achieve a comprehensive understanding of the mechanisms that are responsible for the flow instability.

Experiments were conducted in the IRENav cavitation tunnel on a NACA66-type hydrofoil located at mid-height of the test section, with various angles of attack and coefficient numbers [Astolfi et al., 2000, Leroux and Astolfi, 2003]. A large range of flow configurations was explored, from low cavitating conditions to large cavities characterized by large-scale oscillations and periodical vapour cloud shedding. Simulations have been performed in the same conditions with a numerical model especially developed to compute unsteady cavitating flows [Coutier-Delgosha et al., 2003a]. It solves the RANS equations combined with a physical model of cavitation initially proposed by [Delannoy and Kueny, 1990].

Experimental measurements and numerical results are compared for two angles of attacks of the foil, namely 6° and 8°, which both lead to cloud cavitation. Several flow patterns are detected and discussed hereafter.

1. EXPERIMENTAL DEVICE

The experiments were carried out in the Ecole Navale Cavitation Tunnel, fitted with a 1m long and 0.192 m wide square cross test section (Figure 1). The hydrofoil for this project was of the NACA66 series. The chord length of the hydrofoil was c = 0.150 m and the span was 0.191 m. The relative maximum thickness was τ = 12 % at 45% from the leading edge and the relative maximum camber was 2% at 50 % from the leading edge. Two identical hydrofoils were fabricated. One was equipped with wall-pressure transducers and the second was used for the lift and drag measurements. Except for lift and drag measurements, the hydrofoil were clamped on both sides of the tunnel walls. Pressure measurements were carried out using seventeen piezo-resistive transducers of 10 bars maximum pressure. The transducer locations are given on Fig. 1. As shown, one set of ten transducers was aligned along the chord on the suction side from x/c = 0.05 up to the trailing x/c = 0.90 with a step of 0.10 c from x/c = 0.10. Two sets of three transducers were arranged parallel to this line. One transducer was also mounted on the opposite face in order to analyse the effect on the pressure side of cavitation developing on the suction side. An *in-situ* calibration was performed to take transducer assembly into account. Signals from the wall-pressure transducers were amplified, filtered and collected through a 16 channel, 16-bit A/D digitizer VXI HPE1432A, at simultaneous sample with a maximum available sample frequency of 51.2 kHz. Two nominal sample frequencies, 51.2 kHz and 1.024 kHz, were selected, corresponding to samples of 0.64 s and 4.00 s respectively.

Lift and drag were also measured using a resistive gauge hydrodynamic balance calibrated in our laboratory. The balance was developed for static measurements, however the dynamic response of the balance were also analysed mainly in the case of low frequency pulsation of sheet cavitation. The main effect on the measurements, as it can be expected, is the damping of the intensity of force fluctuations due to the cut-off frequency of the balance. Finally numerical videos were also used to record the cavitating flow at a sample frequency of 25 Hz.

For the experiments, the nominal free stream velocity V_{ref} was 5.33 m/s, corresponding to a Reynolds number based on the foil chord length Re = 0.8 x 10^6. The nominal angles of incidence were successively set to 6° and 8°.

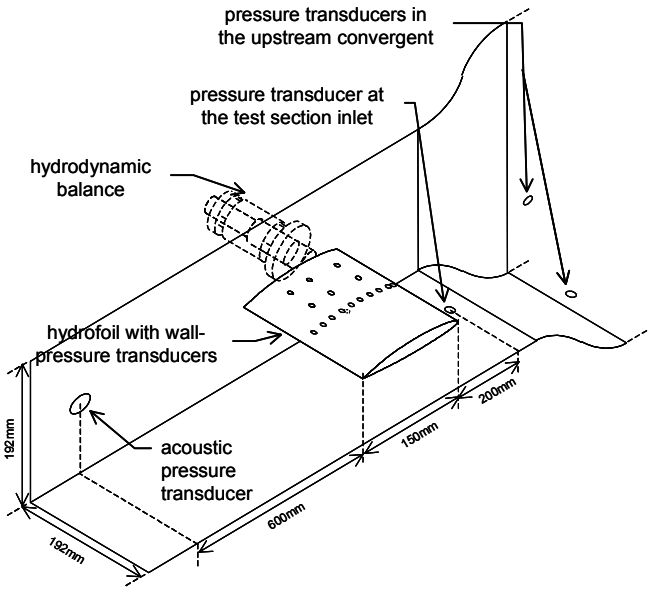

Figure 1. Experimental setting

2. NUMERICAL MODEL

The numerical model solves the unsteady Reynolds averaged Navier-Stokes equations, coupled with a physical model of cavitation. The main features of the solver are given hereafter, and additional details can be found in [Coutier-Delgosha et al., 2003a].

2.1 Physical model of cavitation

The physical model is based on the assumption that the cavitating flow can be considered as a single fluid with varying properties. The fluid is composed of pure liquid at the computational domain inlet, and it becomes a mixture of liquid and vapour in the cavitation areas. So in each cell, the composition of the medium is given by the value of the local void ratio α = vapour vol. / total cell vol., which is directly related to the local non-dimensional density ρ. The void ratio varies from zero (no vapour) to one (pure vapour) as the density decreases from ρ_l (liquid density) to ρ_v (vapour density). This

density is managed by a postulated barotropic state law (Figure 2), which is mainly composed of three parts:

- For a pressure much higher than the vapour pressure p_{vap} (on the right of Figure 2), the flow is composed of pure liquid and the Tait state law [Knapp, 1970] is applied.

- For a pressure much lower than p_{vap}, (on the left of the Figure 2), the fluid is locally completely vaporized and the density is governed by the perfect gas law.

- These two low compressible configurations are joined in the vapour pressure neighbourhood by the central part of the chart, whose high slope models the high compressibility of the liquid/vapour mixture. As a matter of fact, the general shape of this part of the chart has only a little influence on the results: only the value of the minimum celerity of sound C_{min} (i.e. the maximum slope) is relevant. This parameter is thus derived from the estimated value of the celerity of sound in a cavitating area, i.e. about a few meters per second [Jakobsen, 1964]. This consistency with the physical properties of the flow is a major advantage of the model. C_{min} = 1.5 m/s was adopted in [Coutier-Delgosha et al., 2003a] as the default value and it is applied in the present study.

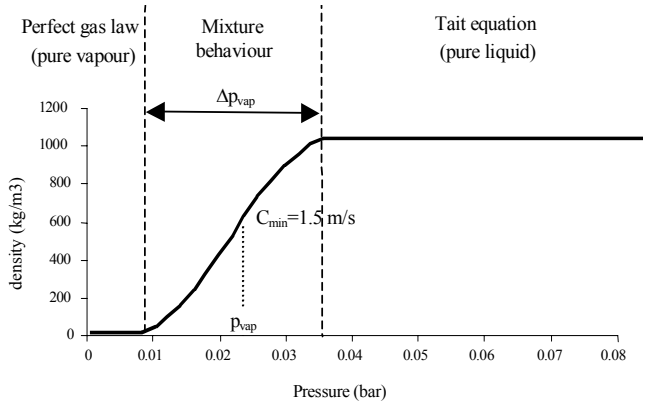

Figure 2. Barotropic state law ρ(P). Water 20°C.

3.2 Numerical resolution

A two-dimensional calculation of the flow around the foil section is performed. As the density depends only on the pressure, thermal effects are neglected and the energy equation is not solved in the present case. The numerical resolution is based on a pressure correction method derived from the SIMPLE algorithm [Patankar, 1981]. The coupling between the Reynolds equations and the highly compressible state law has induced several modifications of the initial scheme [Coutier-Delgosha et al., 2003].

3.3 Turbulence model

As reported in [Yuan and Schnerr, 2001, Coutier-Delgosha et al., 2003a,], simulating cloud cavitation with a standard two-equations turbulence model comes up against serious difficulties, since turbulent dissipation is systematically over-estimated in the rear part of the cavitation sheet. As a result, the re-entrant jet is stopped before breaking the cavity interface, and the flow remains stable. In the case of the physical model applied in the present work, this discrepancy can be related to the compressibility of the two-phase medium. [Coutier-Delgosha et al., 2003b] have shown that taking into account its effects on the turbulence structure, via simple corrections of standard models, leads to a substantial improvement of the simulations.

The modified k-ε RNG turbulence model reported in this previous publication is applied in the computations presented hereafter.

3.4 Boundary conditions, initial conditions, and grid

The classical boundary conditions for incompressible flows are applied: imposed inlet velocity, and fixed outlet pressure.

The numerical process to obtain cavitating conditions is based on the experimental procedure. A first stationary time step is first computed with a high pressure level at the domain outlet, to avoid any flow vaporization. Then, the outlet pressure is decreased slowly during the first hundred time steps, from initial non-cavitating conditions down to reach the desired value of the cavitation number σ. Liquid passing on the foil suction side progressively vaporizes during this decrease. After that the outlet pressure is kept constant and the calculation is continued during 60 T_{ref}, where $T_{ref} = L_{ref}/V_{ref}$ with L_{ref} = 0.15 m the chord length and V_{ref} = 5.33 m/s the inlet flow velocity. So T_{ref} is representative for the transit time of the flow over the foil section. The time step Δt equals T_{ref} / 200. 60 T_{ref} of calculation represent 1.7 s, which is sufficient in the present case to characterize the cavitating flow (oscillation frequency, mean and max. cavity length…).

The computational domain respects as well the geometry of the experimental test section as the foil position. A 630×50 C-type orthogonal mesh is used (Figure 3). Most of the cells are located around the foil, and a contraction of the grid is applied in its upstream part, to obtain an especially fine discretization of the areas where cavitation is expected (Figure 3b). The non-dimensional distance to solid walls y^+ is imposed between 30 and 50, since standard wall functions are applied.

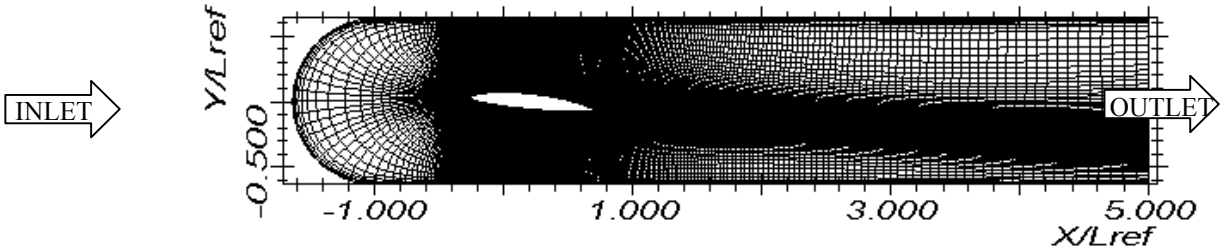

Figure 3. General view of the grid

3. RESULTS

The cavitating flow around the foil has been investigated numerically and experimentally for two angles of attack, namely 6° and 8°. As a matter of fact, these two configurations lead to distinct unsteady periodical behaviours characterised by very different frequencies. The present section is devoted to their description, on the basis of both experimental and numerical results, while section 5 will focus on a detailed investigation of the physical mechanisms involved in the cavity oscillations.

3.1 Qualitative description of the cavity periodical oscillations

For a 8° angle of attack, the cavitation sheet adopts a self-oscillatory behaviour characterized by large vapour cloud sheds.

The Strouhal number based on the max. attached cavity length and the upstream velocity systematically equals 0.3. Figure 4a presents successive flow visualizations of the cavity during one oscillation cycle in the case $\sigma = (P-P_{vap})/(\frac{1}{2}\,\rho V_{ref}^2) = 1.25$: picture one shows the max. cavity (whose length is about 60% of the chord), with the re-entrant jet flowing upstream up to 20% of the chord. On picture 2 this reverse flow cuts the cavity close to the leading edge, which leads (pictures 4 to 6) to cloud cavitation. The cloud is then convected downstream while the cavity starts to grow again (pictures 7 to 9). In all pictures, noticeable wall effects resulting in large vapour structures can be observed along the two lateral sides of the tunnel.

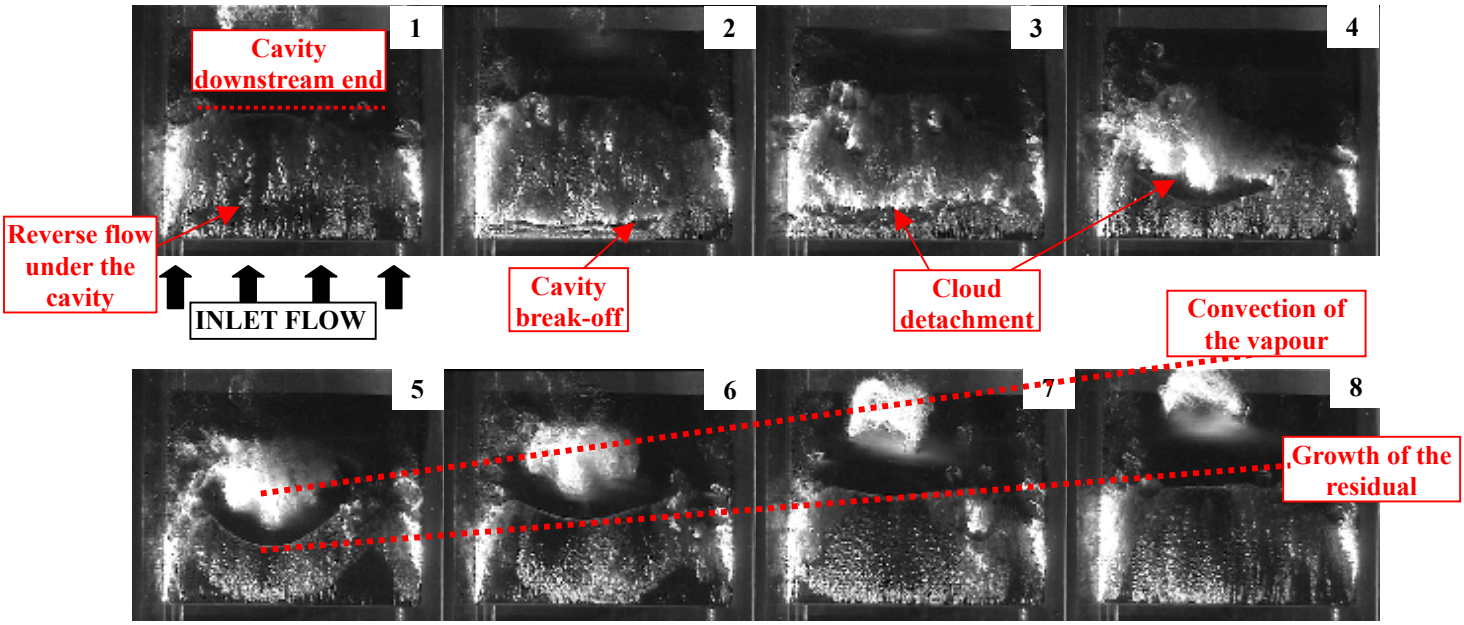

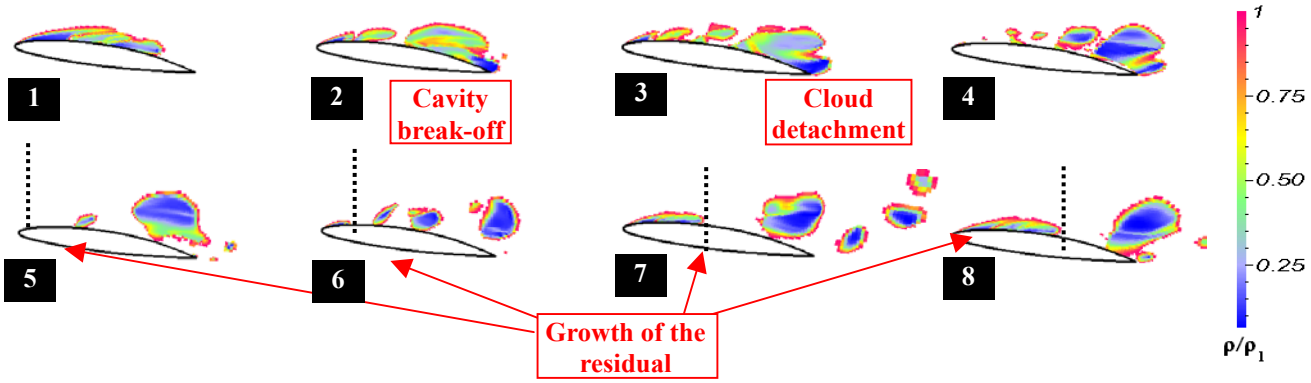

Figure 4a. Top view of the sheet of cavitation during one cycle of self-oscillation behaviour
Experimental flow visualization (Δt = 6.94 ms between two consecutive figures)

Figure 4b. Side view of the sheet of cavitation during one cycle of self-oscillation behaviour
Numerical flow: the colours indicate the density, white for pure liquid and from red to blue when the void ratio increases (Δt = 7 ms between two consecutive figures).
(In both cases, angle of attack 8°, $\sigma = 1.25$, $V_{ref} = 5.33$ m/s)

The entire unsteady process is well predicted by the numerical model, as shown on Figure 4b, which presents the flow density evolution around the foil during one oscillation cycle in the previous flow conditions (σ = 1.3). A good agreement with the experiments is obtained concerning both the self-oscillation frequency and the max. attached cavity length. Moreover, it appears clearly in the numerical results that the re-entrant jet is the main trigger for cloud cavitation: the cavity break-off occurs when it reaches the cavity leading edge and cuts the liquid/vapour interface. The numerical model gives also supplementary indications concerning the structure of the liquid/vapour mixture: the medium is characterized by a rather low void ratio (lower than 0.5) in the main part of the cavity. High void ratio areas – which correspond to the observable cavitation in experiments - can be found only close to the foil.

At 6° angle of attack, a periodical vapour cloud shedding is still observed, but its frequency is considerably lower than previously: the Strouhal number (still based on the max. attached cavity) varies in the range 0.07-0.09, according to the value of the cavitation number σ. Moreover, the cavity behaviour is slightly more complicated: as illustrated on Figure 5a in the case σ = 1.05, two successive steps can be identified. The first one consists in the rapid growth of the cavity up to 50% of the chord (pictures 1 to 4), then a slower growth up to 75% of the chord (pictures 5 to 8) with little vapour shedding in the wake (pictures 9 and 10), and finally the main detachment of the vapour cloud (figure 11). The second step occurs just after this cavity break-off: the growth of the residual cavitation sheet is abruptly stopped by the collapse of the cloud of vapour (picture 12), and the attached cavity almost completely disappears (Figure 13). After that it starts to grow again (pictures 14 and 15). Therefore, this supplementary stage results in a delay before the growing of the next cavity , which explains the significant reduction of the cycle frequency (for this flow conditions, Str= 0.079 is obtained).

Similar cavitating conditions (σ = 1.07) were investigated by calculations (Figure 5b). The periodical behaviour is still well predicted. Both the max. cavity length (80% of the chord, versus 75% in experiments) and the oscillations frequency (Str = 0.09, versus 0.079 in experiments) are close to the measurements. Besides, the secondary vapour emissions (picture 9) and the sudden vanishing of the cavity after the collapse of the vapour cloud (picture 11) are also correctly simulated. However, the computation predicts a larger expansion of the cavity before the collapse than in experiments.

Although the re-entrant jet can never be seen in Figure 5a, the simulations confirm that it is still responsible for the cavity break-off. Figure 6 shows the velocity distribution just before and after the detachment of the vapour cloud. The reverse flow can be observed close to the wall, flowing upstream until its head crosses the limit of the cavitation sheet near the leading edge.

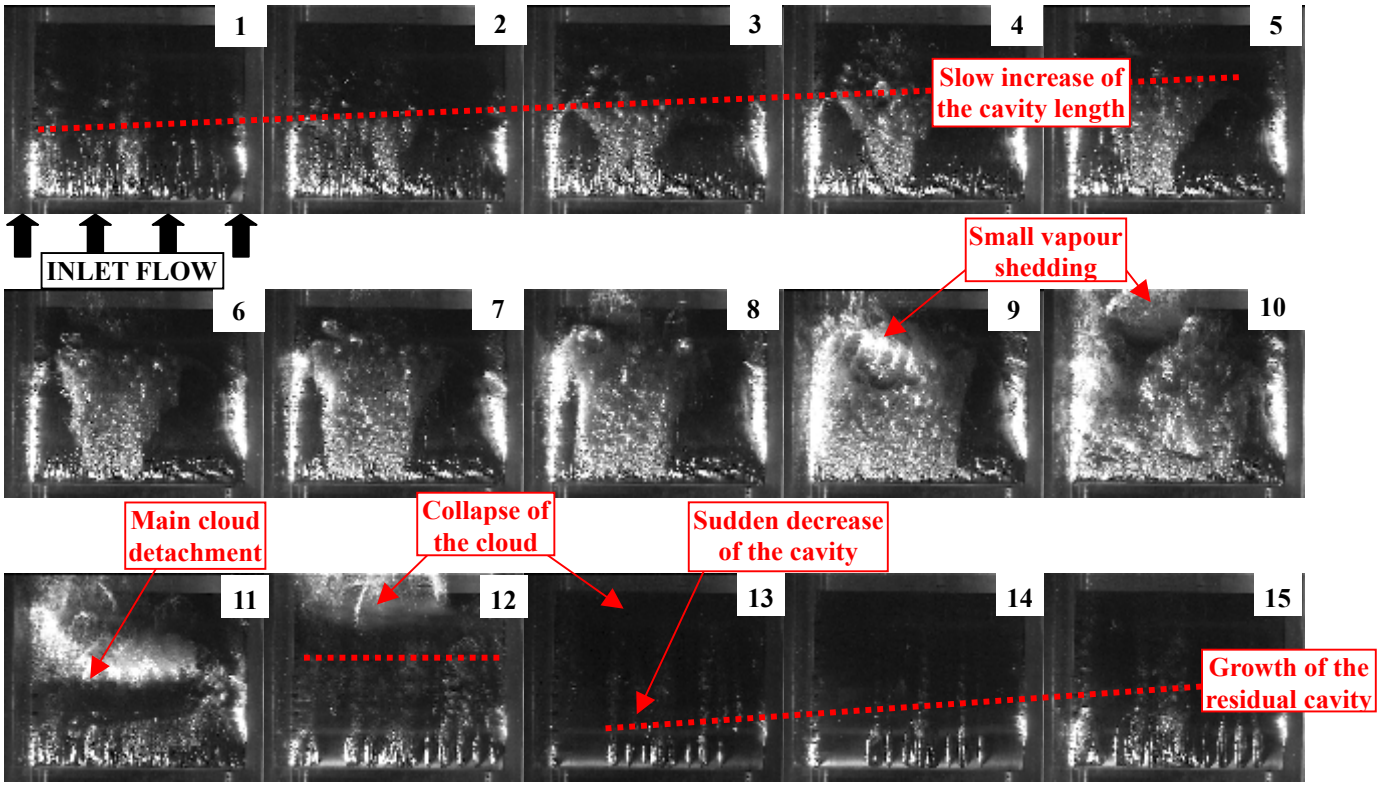

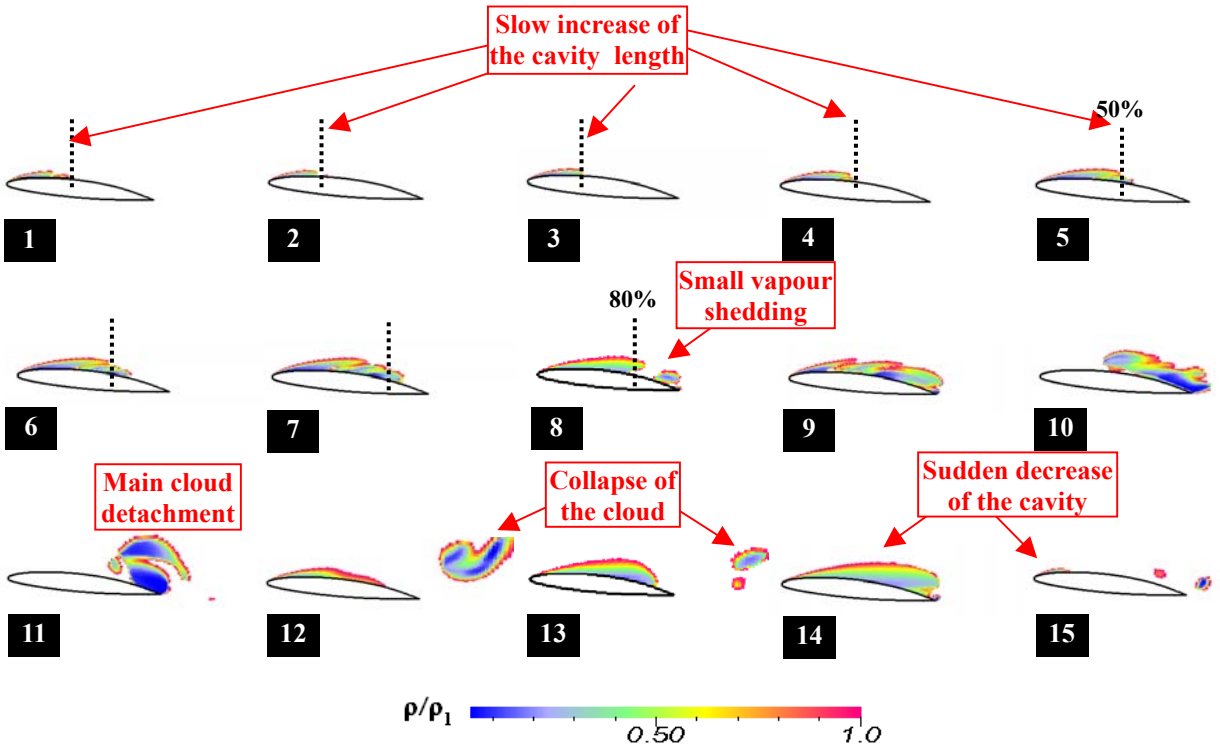

Figure 5. One cycle of the unsteady periodical behaviour at an angle of attack of 6° (V_{ref} = 5.33 m/s)
a) Experimental flow visualization (Top view, Δt = 20 ms between two consecutive figures, σ = 1.05)
b) Numerical flow density (side view, Δt = 20 ms between two consecutive figures, (σ = 1.07)

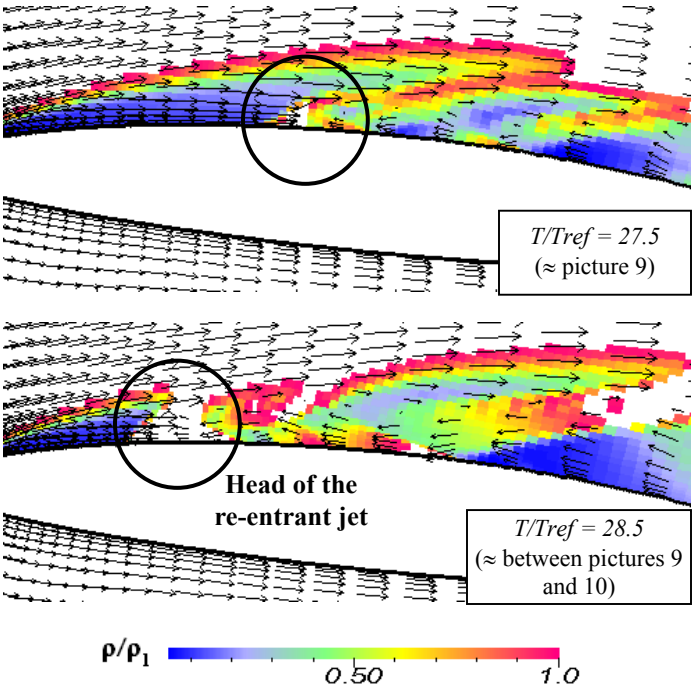

Figure 6. Cavity break-off (zoom of Figure 5b)
(Angle of attack 6°, V_{ref} = 5.33 m/s, σ = 1.07)

3.2 Analysis of the pressure signals

A more quantitative investigation of the periodical behaviours is performed hereafter for a 8° angle of attack and σ = 1.45. Figure 7 shows the time evolution of the pressure fluctuations at mid chord on the foil suction side. Three periods are represented. The pressure fluctuates between low values (corresponding to the presence of vapour) and high values (indicating a pure liquid flow). The sequences one and two correspond respectively to the cavity growth and to the detachment of its rear part. In the present case experimental and numerical results are in good agreement as well concerning the oscillation frequency as the magnitude of the pressure fluctuations.

The evolutions of the lift coefficient given by experiments and calculations are also reported on Figure 7. It shows that the steps of cavity growth correspond to an increase of the foil lift, while the cavity breaks off are responsible for a lift drop. Indeed, the large pressure fluctuations due to the cavity oscillations result in significant variations of the lift coefficient. However, a large discrepancy can be observed between measurements and calculations concerning the magnitude of the fluctuations. This can be attributed to an experimental damping of the intensity of force fluctuations due to the cut-off frequency of the balance.

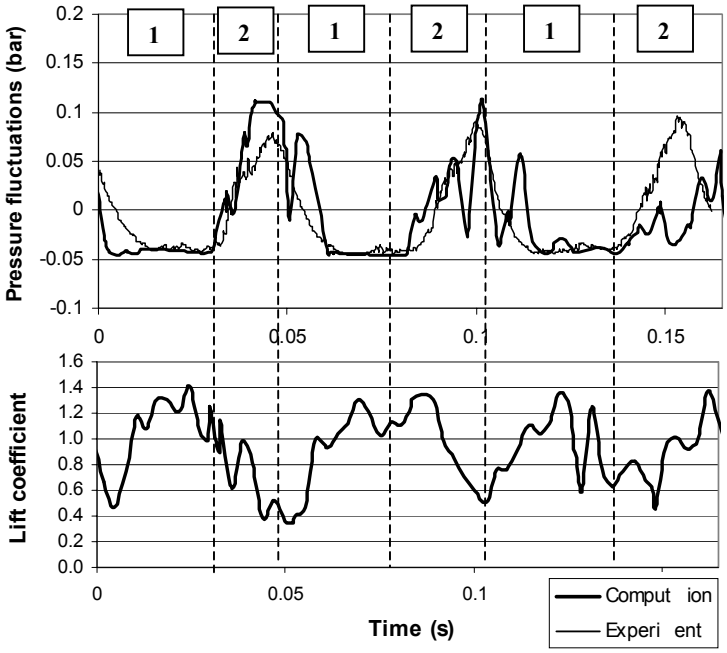

Figure 7. Lift coefficient evolution, and pressure fluctuations at mid chord on the foil suction side
(Angle of attack 8°, $\sigma = 1.45$, $V_{ref} = 5.33$)

A similar analysis is performed at the 6° angle of attack for a cavitation number $\sigma = 1.25$. Two periods of three pressure fluctuations signals are drawn on Figure 8. The three signals correspond to three positions on the foil suction side, respectively 0.3 x/c, 0.5 x/c, and 0.7 x/c. Both experimental and numerical results are reported. Because of the more complex cavity behaviour, four sequences have been identified per period: they correspond respectively to the development of the cavity (1), the cloud detachment (2), the growth of the next cavity (3), and its abrupt vanishing due to the cloud collapse (4). A noticeable discrepancy between experiments and calculations can be observed during sequences 3 and 4: measurements show only a small increase of the cavity before the cloud collapse, so only the sensor located at x/c = 0.3 detects the cavity length fluctuation. The calculation predicts a more important development of the cavity before the cloud collapse, so the three signals report the cavity length increase. This disagreement is mainly due to the fact that the cloud collapse is slightly delayed in the calculation, compared with experiments (see the signal at x/c = 0.3).

The evolution of the lift coefficient is also reported on Figure 8. As previously, the measured fluctuations are much lower than the computed ones. The same effect of the cavity oscillations on the lift coefficient is also obtained: it increases when the sheet of cavitation is growing, and it decreases after the detachment of the vapour cloud. However, the second step of the cycle has almost no influence on the measured lift coefficient, while it considerably affects the computed one. Again, this is due to the longer convection time of the vapour cloud in the calculation, which allows an important development of the cavity before the collapse.

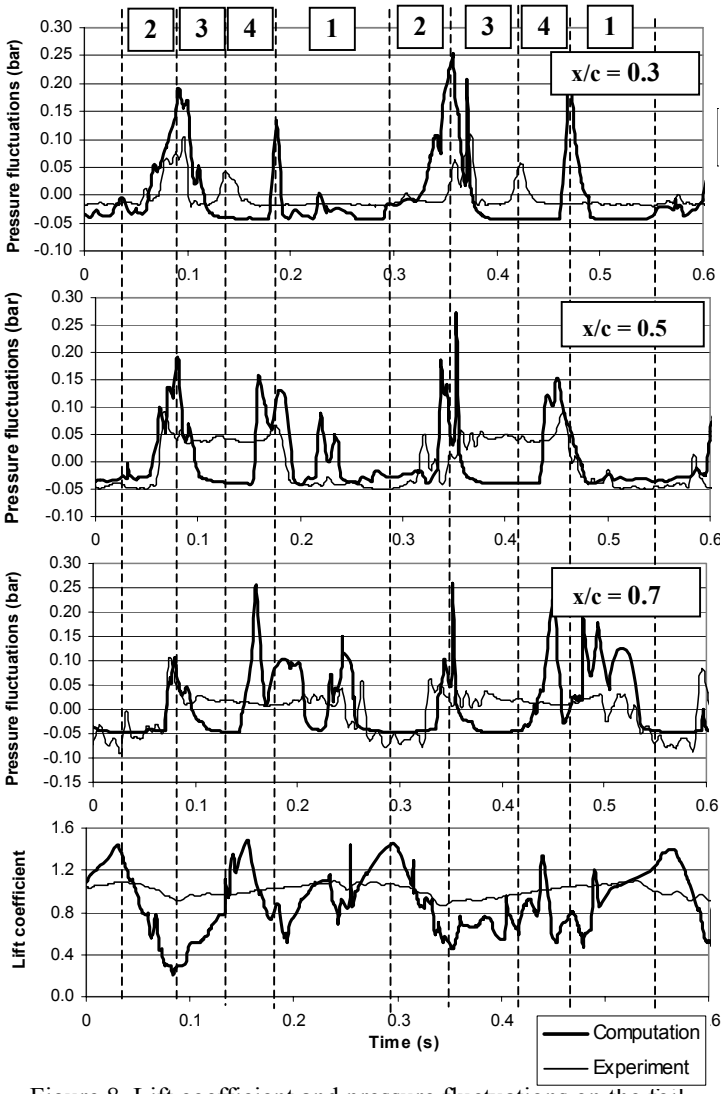

Figure 8. Lift coefficient and pressure fluctuations on the foil suction side at x/c = 0.3, 0.5, 0.7 (6°, $\sigma = 1.25$, $V_{ref} = 5.33$)

4. CONCLUSION

The cavitating flow around a two-dimensional hydrofoil section was investigated in this paper both numerically and experimentally. Two very different cloud cavitation behaviors are obtained at the angles of incidence 8° and 6°. In the first case a periodical cycle including large vapour cloud shedding at Strouhal 0.3 is observed, while in the second case the process is more complex and at lower frequency (Str ≈ 0.08). This frequency drop might result from the difference of magnitude of the pressure wave (figure 9) due to the cloud collapse, which is responsible at 6° for the sudden vanishing of the residual attached cavity. This pressure wave flows upstream from the cloud to the cavity rear part at a velocity close to the local speed of sound: it equals about 900 m/s in the case presented on Figure 9.

It appears that the numerical model is able to predict accurately the two behaviours observed at 6° and 8°. This is a reliable result, since these behaviours are characterized by very different frequencies and different processes. This work is continued currently to improve the quantitative agreement

with experiments and investigate the physical mechanisms during the cloud collapse.

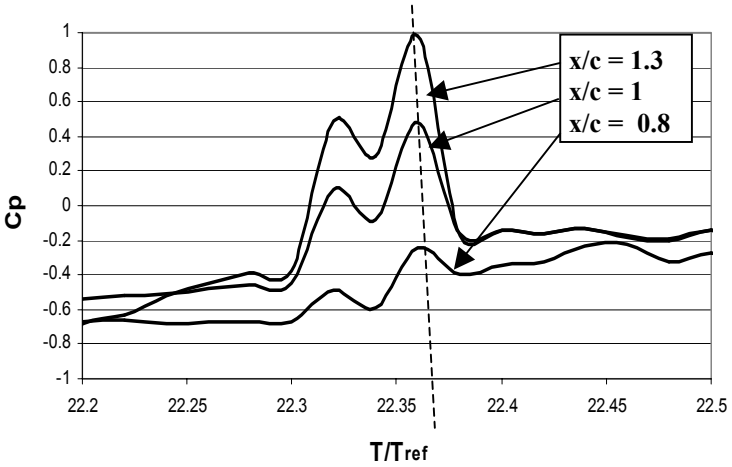

Figure 9. Pressure wave propagation after the cloud collapse. (Angle of attack 6°, $\sigma = 1.25$, $V_{ref} = 5.33$)

ACKNOWLEDGMENTS

Concerning the numerical part of this work, the authors would like to express their gratitude to the CNES (French Space Agency) for its continuous support. The numerical model has been developed for ten years in the LEGI laboratory with successive contributions of Y. Delannoy and J-L. Reboud.

REFERENCES

ARNDT R.E.A., SONG C.C.S., KJELDSEN M., HE J. & KELLER A. 2000 Instability of partial cavitation: a numerical/experimental approach. *Proceedings of the 23rd Symposium on Naval Hydrodynamics*.

ASTOLFI J-A., LEROUX, J-B., DORANGE, P., BILLARD, J-Y., DENISET, F. & DE LA FUENTE, S. 2000 An experimental investigation of cavitation inception and development on a two-dimensional hydrofoil. *J. Ship Res.* **44**(4), 259-269.

COUTIER-DELGOSHA, O., REBOUD, J-L. & DELANNOY, Y. 2003a Numerical simulations in unsteady cavitating flows. *Int. J. for Numerical Methods in Fluids* **42**(5), 527-548.

COUTIER-DELGOSHA, O., FORTES-PATELLA, R. & REBOUD, J-L. 2003b Evaluation of the turbulence model Influence on the Numerical Simulations of Unsteady Cavitation. *J. Fluids Engng.* **125**, 38-45.

COUTIER-DELGOSHA, O., FORTES-PATELLA, R. AND REBOUD, J.L. 2002 Simulation of unsteady cavitation with a two-equations turbulence model including compressibility effects. *J. of Turbulence* **3**, 058, http:\\jot.iop.org.

COUTIER-DELGOSHA, O. & DEVILLERS, J-F. 2003 Experimental and numerical study of the cavitating flow on a hydrofoil. *Proc. 5th Intl Symp. on Cavitation*.

CHEN, Y. & HEISTER, S.D. 1995 Modeling hydrodynamic Non-Equilibrium in Bubbly and Cavitating Flows. *J. Fluids Engng.* **118**(1), 172-178.

KNAPP, R.T., DAILY, J.T., & HAMMIT, F.G. 1970 *Cavitation*. Mc Graw Hill.

DE LANGE, D.F., BRUIN, G.J. & VAN WINJNGAARDEN, L. 1994 On the Mechanism of Cloud Cavitation - Experiment and Modelling. *Proc. 2nd Int. Symp. on Cavitation*, pp. 45-49.

DELANNOY, Y. & KUENY, J.L. 1990 Two-phase flow approach in unsteady cavitation modelling. *Cavitation and Multiphase Flow Forum, ASME-FED* Vol.98, pp. 153-158.

FURNESS, R.A. & HUTTON, S.P. 1975 Experimental and Theoretical Studies of two-dimensional Fixed-Type Cavities. *J. Fluids Engng*. **97**, 515-522.

GROGGER, H.A. & ALAJBEGOVIC, A. 1998 Calculation of the Cavitating Flow in Venturi Geometries Using Two Fluid Model. *Proc. of the Fluids Eng. Div. Summer Meeting*.

JAKOBSEN, J.K. 1964 On the mechanism of head breakdown in cavitating inducers. *J. of basic engineering*, *Transactions of the ASME*, pp. 291-305.

KAWANAMI, Y., KATO, H., YAMAGUCHI, H., TAGAYA, Y. & TANIMURA, M. 1997 Mechanism and control of cloud cavitation. Trans. ASME: *J. Fluids Engng.* **119**, 788-795.

KUBOTA, A, KATO, H. & YAMAGUCHI, H. 1992 A new modelling of cavitating flows: a numerical study of unsteady cavitation on a hydrofoil section. *J. Fluid Mech*. **240**, 59-96.

LABERTEAUX, K.R. & CECCIO, S.L. 2001 Partial cavity flows. Part 1. Cavities forming on models without spanwise variation. *J. Fluid Mech.* **431**, 1-41.

LE, Q., FRANC, J.P. & MICHEL, J.M. 1993 Partial cavities: global behaviour and mean pressure distribution. *J. Fluids Engng.* **115**, 243-248.

LEROUX, J-B. & ASTOLFI, J-A. 2003 An experimental Study of Unsteady Partial Cavitation. *Submitted for publication to the J. Fluids Engng*.

LOHRBERG, H., STOFFEL, B., FORTES-PATELLA, R., COUTIER-DELGOSHA, O. & REBOUD, J-L. 2002 Numerical and experimental investigation on the cavitating flow in a cascade of hydrofoils. *Experiments in Fluids* **33**(4), 578-586.

LUSH, P.A. & PETERS, P.I. 1982 Visualisation of the cavitating flow in a Venturi Type Duct using High-Speed Cine Photography. *Proc. IAHR Conf. on operating problems of pump stations and power plants*.

MERKLE, C.L., FENG, J. & BUELOW, P.E.O. 1998 Computational modelling of the dynamics of sheet cavitation**.** *Proc. 3rd Intl. Symp. on Cavitation,*, Vol. 2, pp. 307-314.

PATANKAR, S.V. 1981 *Numerical heat transfer and fluid flow*. Hemisphere Publishing Corporation.

PHAM, T.M., LARRARTE, F. & FRUMAN, D.H. 1999 Investigation of Unsteady Sheet Cavitation and Cloud Cavitation Mechanisms. *J. Fluids Engng.* **121**, 289-296.

SONG, C.C.S. & QIN, Q. 2001 Numerical simulation of unsteady cavitating flow. Proc. 4th Intl Symp. on Cavitation.

STUTZ, B. & REBOUD, J-L. 1997a Experiments on Unsteady Cavitation. *Experiments in Fluids* **23**, 191-198.

STUTZ, B. & REBOUD, J-L. 1997b, Two-phase flow structure of sheet cavitation. *Phys. Fluids* **9**(12), 3678-3686.

YUAN W & SCHNERR G. H. 2002 Optimization of two-phase flow in injection nozzles – Interaction of cavitation and external jet formation. *Proc. of ASME Fluids Eng. Summer Meeting*.